

New Physics/Resonances in Vector Boson Scattering at the LHC

JÜRGEN REUTER^{1a}, WOLFGANG KILIAN^{2b}, THORSTEN OHL^{3c}, MARCO SEKULLA^{4d}

^a*DESY Theory Group, D-22603 Hamburg, Germany*

^b*Department of Physics, University of Siegen, D-57068 Siegen, Germany*

^c*Faculty of Physics and Astronomy, Würzburg University, D-97074 Würzburg, Germany*

^d*Institute for Theoretical Physics, Karlsruhe Institute of Technology, D-76128 Karlsruhe, Germany*

Talk given at the "Conference on New Physics at the Large Hadron Collider", 29.02. - 04.03.2016, Nanyang University, Singapore

ABSTRACT

Vector boson scattering is (together with the production of multiple electroweak gauge bosons) the key process in the current run 2 of LHC to probe the microscopic nature of electroweak symmetry breaking. Deviations from the Standard Model are generically parameterized by higher-dimensional operators, however, there is a subtle issue of perturbative unitarity for such approaches for the process above. We discuss a parameter-free unitarization prescription to get physically meaningful predictions. In the second part, we construct simplified models for generic new resonances that can appear in vector boson scattering, with a special focus on the technicalities of tensor resonances.

¹juergen.reuter@desy.de

²kilian@physik.uni-siegen.de

³ohl@physik.uni-wuerzburg.de

⁴marco.sekulla@kit.edu

1 Motivation

Run I of the LHC has not only revealed a Standard Model-like Higgs boson [1,2] together with measuring its mass and some of its properties and couplings, but also established the scattering process of electroweak gauge bosons[3,4,5] (VBS) as predicted by the Standard Model (SM). This process gives insights in the nature of the electroweak symmetry breaking (EWSB) sector and further fundamental properties of the Higgs. In the SM, the electroweak breaking sector is described as a weakly interacting theory, where the Higgs boson is strongly suppressing the vector boson scattering process at high center-of-mass energies and the scattering amplitude is dominated by the transversal vector boson scattering.

Without the Higgs the VBS scattering amplitudes $VV \rightarrow VV$, where V is W^\pm, Z , will rise with s/v^2 due to the dominant contribution of scalar Goldstone-boson scattering, which represents the longitudinal degrees of freedom of the vector boson scattering. The electroweak interactions would become strongly interacting in the TeV range. However, the initial limits on VBS are rather weak and only scales close to the pair-production threshold of ~ 200 GeV are probed. Run II and III of the LHC and future (high-energy) e^+e^- colliders will improve the accuracy and provide new insights in the origin of EWSB. The delicate cancellation between the EW gauge bosons and the Higgs boson in VBS, makes this channel an ideal, though not easy place to search for new physics.

The discussion in these proceedings is based on our publications in [6,7,8,9].

2 Effective Field Theory, Perturbative Unitarity and Unitarization

To study new physics in the VBS process generically, we will use the framework of Effective Field Theories (EFT). A set of higher dimensional operators extends the SM Lagrangian to quantify deviations from the SM, which originate from some new physics at a high energy scale Λ_i as

$$\mathcal{L} = \mathcal{L}_{SM} + \sum_i \frac{C_i}{\Lambda_i^{d-4}} \mathcal{O}^d. \quad (1)$$

Here, C_i are the associated Wilson coefficients of the operators. Due to lack of knowledge of both parameters, we introduce the ratio coupling $F_i = \frac{C_i}{\Lambda_i^{d-4}}$.

Many different operator bases have been proposed for the electroweak sector, an overview and also translations between them have been discussed e.g. in [10,11]. Here, for illustrative purposes, we take just two different operators, \mathcal{O}_{HD} as a dim-6 operator, and the two dim-8 operators, $\mathcal{O}_{S,0}$ and $\mathcal{O}_{S,1}$. All of these operators could arise easily in popular scenarios of new physics beyond the SM (BSM) like Composite Higgs, Little Higgs or Extra Dimensions. The LHC experiments are studying all of three of them to gain sensitivity in various channels like

dibosons, tribosons, precision Higgs data and VBS. The operators are given by

$$\mathcal{L}_{HD} = F_{HD} \text{tr} \mathbf{H}^\dagger \mathbf{H} - \frac{v^2}{4} \cdot \text{tr} (\mathbf{D}_\mu \mathbf{H})^\dagger (\mathbf{D}^\mu \mathbf{H}), \quad (2)$$

$$\mathcal{L}_{S,0} = F_{S,0} \text{tr} (\mathbf{D}_\mu \mathbf{H})^\dagger \mathbf{D}_\nu \mathbf{H} \cdot \text{tr} (\mathbf{D}^\mu \mathbf{H})^\dagger \mathbf{D}^\nu \mathbf{H}, \quad (3)$$

$$\mathcal{L}_{S,1} = F_{S,1} \text{tr} (\mathbf{D}_\mu \mathbf{H})^\dagger \mathbf{D}^\mu \mathbf{H} \cdot \text{tr} (\mathbf{D}_\nu \mathbf{H})^\dagger \mathbf{D}^\nu \mathbf{H}. \quad (4)$$

Due to the unknown microscopic picture of the underlying energy giving rise to these operators, the validity range of the EFT is also a priori unknown. In this case, the unitarity condition is used to determine the validity of the EFT.

In the left-hand side of Fig. 1, the cross section for the complete LHC process $pp \rightarrow W^+W^+jj$ at leading order – computed using the Monte-Carlo generator WHIZARD with CTEQ6L

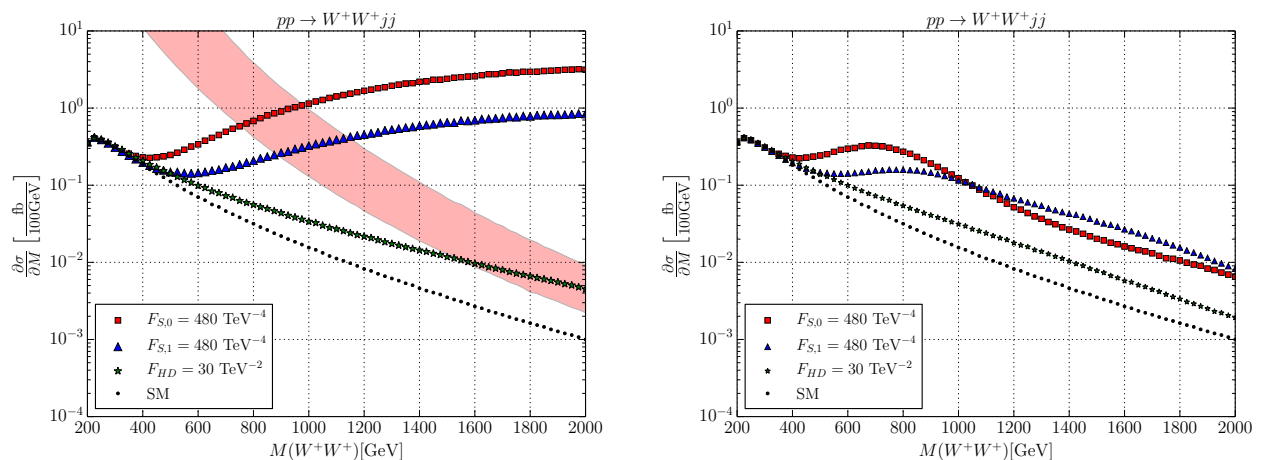


Figure 1: $pp \rightarrow W^+W^+jj$, left: naive EFT results that violate unitarity, QCD contributions neglected. The band describes maximal allowed values, due to unitarity constraints, for the differential cross section. The lower bound describes the saturation of \mathcal{A}_{20} and the upper bound describes the simultaneous saturation of \mathcal{A}_{20} and \mathcal{A}_{22} , right: unitarized result. Cuts: $M_{jj} > 500$ GeV; $\Delta\eta_{jj} > 2.4$; $p_T^j > 20$ GeV; $|\eta_j| > 4.5$.

PDF sets – is shown. The SM curve is compared to three curves for models which contain a single nonzero coefficient for the three different effective higher dimensional operators, respectively. For an indication of the unitarity limits, we have included a quartic Goldstone interaction amplitude with a constant coefficient $a_{IJ} = i$ in the $I = 2$ and $J = 0, 2$ isospin and spin channels and recomputed the process with this modification. The Goldstone boson scattering amplitudes are very good approximations to the scattering of longitudinal EW gauge bosons by means of the Goldstone boson equivalence theorem. By projecting the partial waves into their spin and isospin components, the optical theorem is used to determine the condition for perturbative unitarity in the same way as in [12]. Further details are listed in [7]. At high invariant mass M_{VV} of the WW -scattering system, the enhancement the crosssection by $\frac{M_{WW}^8}{m_H^8}$ in comparison to the SM due to the dimension eight operators are dominant. The coefficients of the higher

dimension operators are chosen within current LHC bounds. We concentrated to the like-sign WW scattering as this is the clearest channel at the LHC with the smallest backgrounds. It only appears in the isospin two channel. In the light red band, we plotted the unitarity limit by demanding that the \mathcal{A}_{20} and \mathcal{A}_{22} for isospin two and spin zero and two, respectively, are saturated, i.e. reaching their maximal value of 32π allowed by perturbative unitarity.

The prediction of the dimension eight operators violate the unitarity limit and become unphysical in an energy regime, which can be tested at the LHC. Naively, one could introduce a cut-off to forbid these unphysical events manually (a prescription also partially used by ATLAS and CMS, known as 'event clipping'). Such a cutoff could also be motivated theoretically by the argument that these events could have never arisen in a UV-complete theory. However, this leads to a sharp edge in the distribution (at level of the vector bosons) which does not resemble any sensible approximation to a UV-complete theory, and furthermore there are also experimental constrictions for doing so: In case of the W^+W^+ scattering, the final state includes two neutrinos and the WW invariant mass cannot be experimentally reconstructed. Other methods to treat this high-energy regime are by means of so-called form factors which, however, depend on at least two arbitrary parameters, the exponent of the momentum dependence in the denominator (the 'multipole' parameter) and the cutoff scale which a priori has nothing to

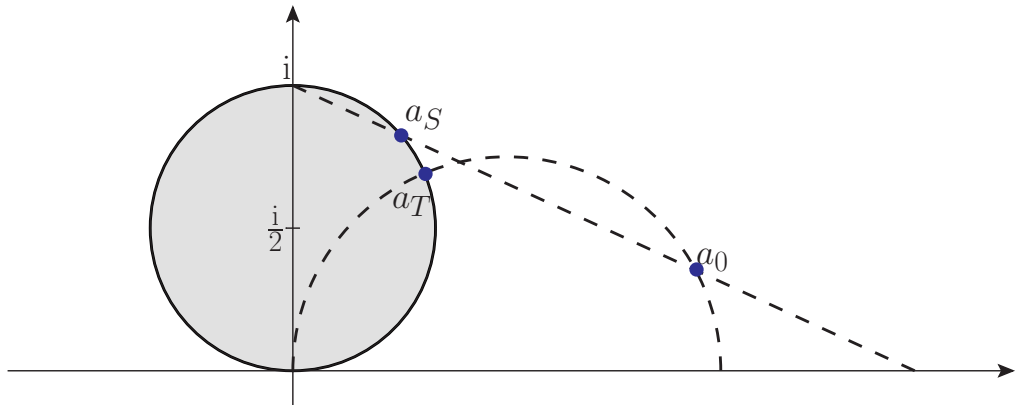


Figure 2: *Geometrical representation: stereographic projection vs Thales projection.*

do with the scale Λ appearing in front of the Wilson coefficients.

In order to have a meaningful description that does not depend on any parameters lacking physical motivation, we introduce the T -matrix unitarization scheme (cf. Fig. 2) as a general extension of the K -matrix unitarisation to provide event samples, which satisfy the unitarity bound. The T -matrix scheme is applicable for cases where the amplitude has an imaginary part itself already, and is also defined without relying on a perturbative expansion. For more details cf. [7]. The right-hand side of Fig. 1 shows the damping of the cross sections for high energies due to the saturation of the amplitudes. The T -matrix scheme is only one extrapolation for possible high energy scenarios. All physical scenarios have to fulfill the unitarity condition which is graphically represented by the Argand circle. If no new physics is involved in the electroweak sector, the elastic scattering amplitude of the Standard model will stay at the origin on the bottom of the Argand circle (Fig. 3a). If the EFT is naively added, amplitudes start to rise

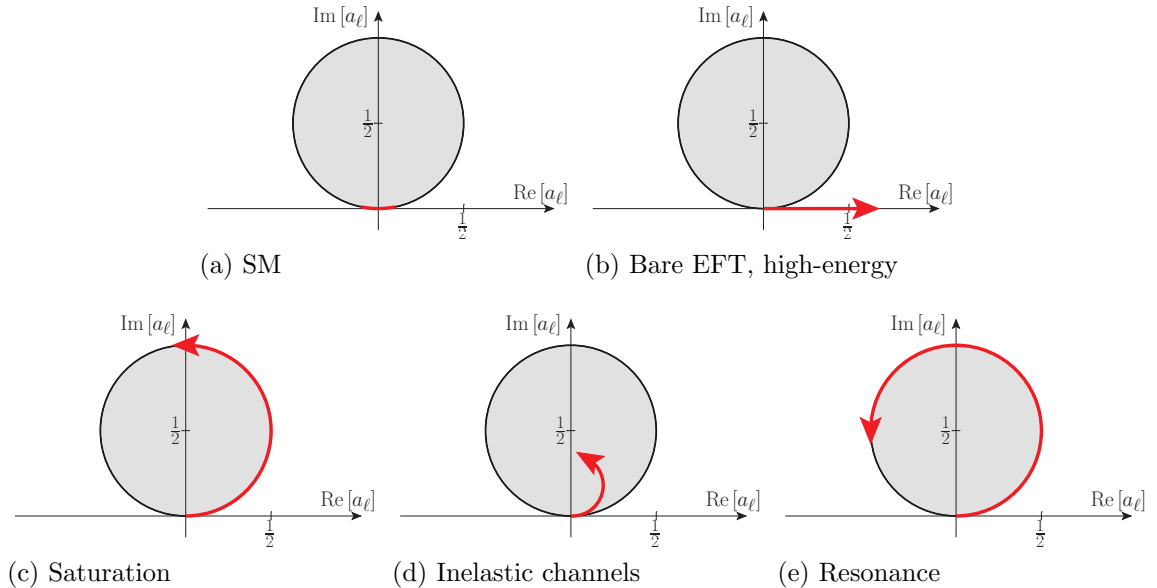


Figure 3: Possible situations for scattering amplitudes respecting the Argand circle.

and will leave the Argand circle to finally violate unitarity (cf. Fig. 3b, as there are new degrees of freedom in the strict EFT, the amplitude can never develop an imaginary part to return to the Argand circle). To remedy this unphysical behavior of the amplitude, unitarization prescriptions are introduced to project the amplitude back onto the Argand circle. T-matrix unitarization saturates the amplitude, in the sense that it is equivalent to an infinitely broad resonance at infinity, similarly to a strongly interacting continuum present over an extended range in momentum space. Another option to correct the unphysical EFT prediction is using the form-factor scheme, a possible case of entering the inelastic regime with additional channels opening up (cf. Fig. 3d). A third approach would be the addition of additional resonances (either weakly or strongly coupled), which could be (part of the) origin for the dim-8 operators (cf. Fig. 3e). Here, the amplitude will ideally fall again beyond the resonance, but could show a rise again due to continuum contributions or the onset of a further resonance.

3 Resonances and Simplified Models

As the LHC is intended to be a discovery machine, it might be advantageous to assume that a new resonance or particle might be within the kinematic reach of the machine, especially given the high amount of luminosity to be collected in runs II and III. In order to be as general as possible in studying what kind of resonances could show in vector boson scattering – specific models would be Two-Higgs double models, including the (N)MSSM, Composite Higgs, Little Higgs (for limits cf. e.g. [13]), Twin Higgs, etc. – we classify all resonances that can couple to the electroweak diboson systems according to their spin and isospin quantum numbers. For simplicity, we neglect couplings to photons, but of course they are present due to EW

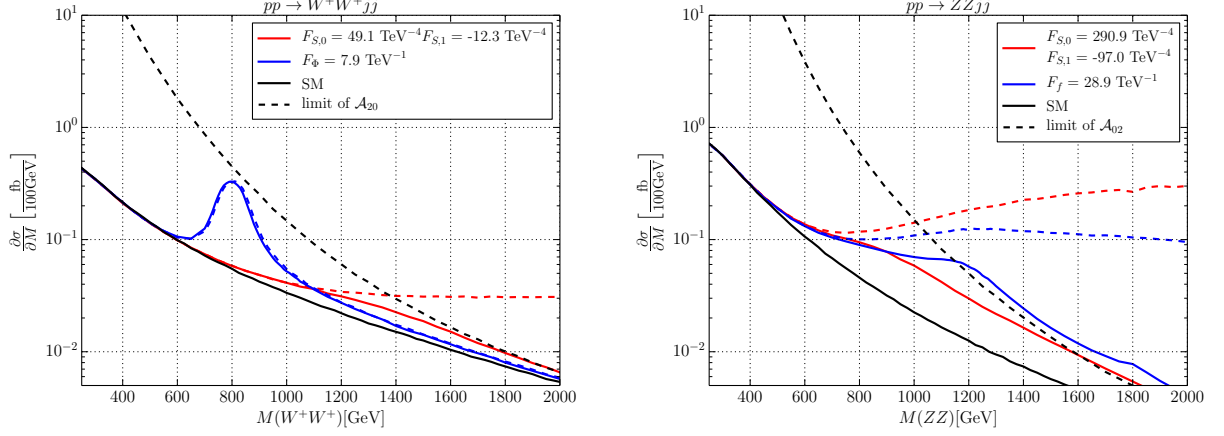


Figure 4: *Differential cross sections of a scalar-isotensor resonance (left) and an isoscalar-tensor resonance (right). Solid line: unitarized results, dashed lines: naive result, black dashed line: limit of saturation of \mathcal{A}_{22} (W^+W^+) / \mathcal{A}_{02} (ZZ). Cuts: $M_{jj} > 500$ GeV; $\Delta\eta_{jj} > 2.4$; $p_T^j > 20$ GeV; $|\eta_j| > 4.5$. Left: $pp \rightarrow W^+W^+jj$, scalar-isotensor with $m_\phi = 800$ GeV and $\Gamma_\phi = 80$ GeV, right: $pp \rightarrow ZZjj$, strongly interacting isotensor scalar with $m_f = 1200$ GeV and $\Gamma_f = 480$ GeV.*

gauge invariance. These possible resonances can be categorized in terms of the approximate $SU(2)_L \times SU(2)_R$, which is a good approximation for weak boson scattering, and the spin. The $(0,0)$ and the $(1,1)$ representation of the $SU(2)_L \times SU(2)_R$ are abbreviated as isoscalar and isotensor, respectively. We can distinguish the resonances for elastic vector boson scattering into a isoscalar scalar σ , a isoscalar tensor f , a isotensor scalar ϕ and a isotensor tensor X . The interaction with longitudinal vector bosons is modeled by the following currents:

$$J_\sigma = F_\sigma \text{tr}(\mathbf{D}_\mu \mathbf{H})^\dagger \mathbf{D}^\mu \mathbf{H}, \quad (5a)$$

$$J_\phi = F_\phi \left((\mathbf{D}_\mu \mathbf{H})^\dagger \otimes \mathbf{D}^\mu \mathbf{H} + \frac{1}{8} \text{tr}(\mathbf{D}_\mu \mathbf{H})^\dagger \mathbf{D}^\mu \mathbf{H} \right) \tau^{aa}, \quad (5b)$$

$$J_f^{\mu\nu} = F_f \left(\text{tr}(\mathbf{D}^\mu \mathbf{H})^\dagger \mathbf{D}^\nu \mathbf{H} - \frac{c_f}{4} g^{\mu\nu} \text{tr}(\mathbf{D}_\rho \mathbf{H})^\dagger \mathbf{D}^\rho \mathbf{H} \right), \quad (5c)$$

$$J_X^{\mu\nu} = F_X \left[\frac{1}{2} \left((\mathbf{D}^\mu \mathbf{H})^\dagger \otimes \mathbf{D}^\nu \mathbf{H} + (\mathbf{D}^\nu \mathbf{H})^\dagger \otimes \mathbf{D}^\mu \mathbf{H} \right) - \frac{c_X}{4} g^{\mu\nu} (\mathbf{D}_\rho \mathbf{H})^\dagger \otimes \mathbf{D}^\rho \mathbf{H} \right. \\ \left. + \frac{1}{8} \left(\text{tr}(\mathbf{D}^\mu \mathbf{H})^\dagger \mathbf{D}^\nu \mathbf{H} - \frac{c_X}{4} g^{\mu\nu} \text{tr}(\mathbf{D}_\rho \mathbf{H})^\dagger \mathbf{D}^\rho \mathbf{H} \right) \right] \tau^{aa}. \quad (5d)$$

Here, $\mathbf{H} = \frac{1}{2}(\mathbf{1}(v + H) - iw^a \tau^a)$, and τ^{aa} is the tensor-product representation for the isotensor case. With those resonances at hand, parameterized simply by their masses and widths, together with the currents above, one can integrate them out again and derive the corresponding Wilson coefficients of the dim-8 operators $\mathcal{O}_{S,0}$ and $\mathcal{O}_{S,1}$ in the section before, for all resonances considered above. The coefficients are listed in the following table, in units of $32\pi\Gamma/M^5$:

	σ	ϕ	f	X
$F_{S,0}$	$\frac{1}{2}$	2	15	5
$F_{S,1}$	–	$-\frac{1}{2}$	-5	-35

Tensor resonances as they could arise as Kaluza-Klein recurrences of a higher-dimensional gravity theory, but also as analogues to tensor mesons in a composite model, are particularly interesting. They usually give the largest signal contributions, as here the maximum number of spin components are involved in the scattering, namely five, compared to scalar and vector cases. There is a substantial difference in the theoretical handling of those intrinsic spin degrees of freedom when dealing with the tensor resonance on-shell and off-shell. In a full Monte-Carlo simulation (cf. below), one actually simulates the final state and always has the tensor resonance in off-shell configurations. Using the analogue of unitarity gauge for tensors, the propagators lead to a bad high-energy behavior of the amplitudes. Of course, these could again be treated by a unitarization prescription, however, it is better to cure most of these issues beforehand. A symmetric tensor field $f_{\mu\nu}$ has 10 components which are reduced by the on-shell conditions to five physical components. These conditions are the tracelessness, $f_{\mu}{}^{\mu} = 0$ and the transversality, $\partial_{\mu}f^{\mu\nu} = 0$. The original formulation using the Fierz-Pauli Lagrangian [14] is not valid off-shell, so we use the Stückelberg mechanism [15,16] to make the off-shell high-energy behavior explicit. Onshell, there is only the tensor field, $f^{\mu\nu}$, while off-shell there is a vector field, $A^{\mu} \sim \partial_{\nu}f^{\mu\nu}$, which corresponds to the transversality condition, a scalar implementing the fully contracted transversality, $\phi \sim \partial_{\mu}\partial_{\nu}f^{\mu\nu}$, and another scalar corresponding to the tracelessness, $\sigma \sim f_{\mu}{}^{\mu}$. By gauge fixing, one of the scalar degrees of freedom is redundant: $\sigma = -\phi$. The technical details together with the full Lagrangians and currents for the Fierz-Pauli as well as the Stückelberg picture can be found in [7].

Fig. 4 shows two examples how differential invariant mass distributions of the diboson system behave at the LHC in the presence of such resonances. Both plots show different resonances in different scenarios: the left plot a narrow isotensor scalar with mass $m_{\phi} = 800$ GeV and width $\Gamma_f = 80$ GeV, the right one a strongly-interacting scenario with a broad isoscalar-tensor resonance of mass $m_f = 1.2$ TeV and width $\Gamma_f = 480$ GeV. The left plot shows the like-sign W^+W^+ channel, the right one the opposite-sign $W^+W^- \rightarrow ZZ$ channel, respectively. General cuts for selection and signal/background enhancement are shown in the caption. The full black line is the SM, the black dashed line shows the corresponding unitarity limit of the leading partial wave amplitude, the full blue line shows the SM with the corresponding resonance, while full red line depicts the approximation with the two Wilson coefficients, $F_{S,0}$ and $F_{S,1}$. Clearly, if explicit resonances are in the kinematic reach of the LHC, the EFT is no longer a viable approximation in any case. Note that even in the simulation with an explicit resonance, T-matrix unitarization has been applied to unitarize the high-energy tail of the distribution. As here the amplitudes do have explicitly complex poles, T-matrix unitarization is actually needed.

We have implemented the complete set of dim-6 operators as well as a complete set of bosonic dim-8 operators together with the prescription of K-/T-matrix unitarization (for longitudinal VBS) in the Monte Carlo event generator WHIZARD [17,18]. It contains a quite elaborate

machinery for QCD precision physics, where it uses the color flow formalism [19], it has its own parton shower implementations [20], and quite recently has successfully demonstrated its QCD NLO capabilities [22]. WHIZARD has been used for a plethora of BSM studies, and is able to read in external models, e.g. via [21]. Using this implementation, we simulated vector boson scattering at the LHC with its design energy of $\sqrt{s} = 14$ TeV for all kinds of narrower and wider resonances of different spin and isospin. Fig. 5 shows an example of a isoscalar tensor resonance

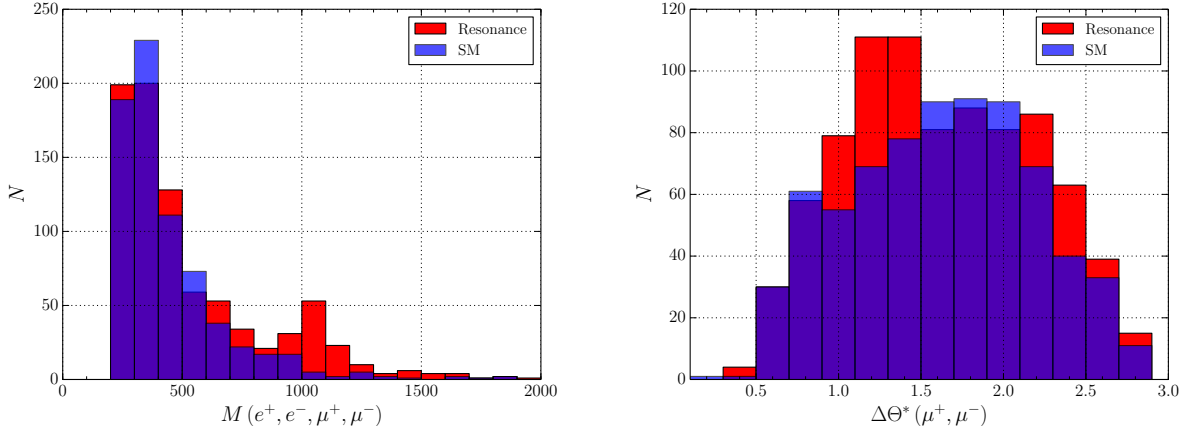


Figure 5: *Isoscalar-tensor resonance at $m_f = 1000$ GeV and $\Gamma_f = 100$ GeV $pp \rightarrow e^+e^-\mu^+\mu^-jj$ at $\sqrt{s} = 14$ TeV with luminosity of 3000 fb^{-1} , with cuts $M_{jj} > 500$ GeV; $\Delta\eta_{jj} > 2.4$; $p_T^j > 20$ GeV; $|\eta_j| > 4.5$; $100 \text{ GeV} > M_{e^+e^-} > 80$ GeV; $100 \text{ GeV} > M_{\mu^+\mu^-} > 80$ GeV.*

of mass $m_f = 1$ TeV and a width of $\Gamma_f = 100$ GeV in the scattering of opposite-sign W s into two Z s. A standard set of selection cuts are mentioned in the caption of the figure. The left plot shows the invariant mass of the diboson system, which in this case is fully reconstructible, while the right plot shows the distribution of the opening angle of the two muons from one of the Z s. The latter is one of the angular observables that could be used to discriminate the spin of such resonances. More examples can be found in [7].

4 Conclusions

The search for new physics in the electroweak in vector boson scattering at the LHC can be studied in the context of effective field theory, however, the introduction of dim-6 and dim-8 operators leads to a very limited range of applicability of the EFT ansatz. In many models, dim-8 operators could be the leading contributions where tree-level effects are forbidden by symmetries, and first contributions come in at the one-loop level, i.e. at dim-8. LHC as a hadron collider probes a vast range of energy scales, and high-energy events tend to (over-)dominate the exclusion limits (or search potentials) for new models. In most cases this is due to wrong assumptions on the underlying model, if EFT-based approaches in regimes are used where perturbative unitarity is lost. We studied examples of a dim-6 and two dim-8 operators and derived unitarity limits for the different spin and isospin channels in the scattering of

transverse electroweak vector bosons. Then, a unitarization method, T-matrix unitarization, that is parameter-free and that is an extension of the "classic" K-matrix unitarization has been applied to produce results that are physically meaningful. The T-matrix unitarization has certain advantages, as it is defined for amplitudes that are intrinsically complex, and does not rely on the existence of a perturbative expansion. For weakly coupled amplitudes without imaginary parts it is identical to K-matrix unitarization. This procedure is not just an academic exercise, it allows to produce Monte Carlo events that could actually come from a quantum field theory realized in nature. Furthermore, it is itself a possible limit of a limit with a strongly interacting continuum like in QCD or close to a quasi-conformal fixed point, or it could correspond to a strongly interacting model right below the onset of a new resonance that is just a little bit outside the kinematical reach of LHC. We show examples of cross sections as well as kinematic and angular distributions to show the effects between "bare" EFT and unitarized simulations. Beyond this parameter-less approach to new physics in vector boson scattering, we provided a set of simplified models taking the SM added by all possible resonances in the spin-isospin channels to which two EW vector bosons can couple. We focused on scalar and tensor resonances, while vector resonances are more complicated due to their potential mixing with the EW bosons. To account for effects of particularly strongly interacting models, in addition higher-dimensional operators can be added. Also, adding just single resonances does not lead to renormalizable models with sound high-energy behavior, hence, we also applied T-matrix unitarization to the simplified models. In order to start with a prescription that already has the best possible high-energy behavior, we isolated the scalar and vector degrees of freedom in massive tensor fields via the Stückelberg mechanism to represent explicitly the bad behavior of tensor propagators in unitarity gauge. We concluded with a fully differential example for a simplified model with an isoscalar tensor resonance. Further work will be devoted to the study of transverse W and Z polarizations, the discussion of vector resonances as well as VBS at future lepton colliders [23,24]. An old study of the ILC capabilities [25] will be updated soon [26].

Acknowledgements

JRR wants to thank the organizers and particularly Harald Fritzsch for the invitation, for the local support and the excellent organization at a great venue.

References

- [1] G. Aad *et al.* [ATLAS Collaboration], Phys. Lett. B **716**, 1 (2012) doi:10.1016/j.physletb.2012.08.020 [arXiv:1207.7214 [hep-ex]].
- [2] S. Chatrchyan *et al.* [CMS Collaboration], Phys. Lett. B **716**, 30 (2012) doi:10.1016/j.physletb.2012.08.021 [arXiv:1207.7235 [hep-ex]].
- [3] G. Aad *et al.* [ATLAS Collaboration], Phys. Rev. Lett. **113**, no. 14, 141803 (2014) [arXiv:1405.6241 [hep-ex]].

- [4] The ATLAS collaboration [ATLAS Collaboration], ATLAS-CONF-2014-013.
- [5] CMS Collaboration [CMS Collaboration], CMS-PAS-FSQ-13-008.
- [6] A. Alboteanu, W. Kilian and J. Reuter, JHEP **0811**, 010 (2008) [arXiv:0806.4145 [hep-ph]].
- [7] W. Kilian, T. Ohl, J. Reuter and M. Sekulla, Phys. Rev. D **91** (2015) 096007 [arXiv:1408.6207 [hep-ph]].
- [8] W. Kilian, T. Ohl, J. Reuter and M. Sekulla, Phys. Rev. D **93**, no. 3, 036004 (2016) doi:10.1103/PhysRevD.93.036004 [arXiv:1511.00022 [hep-ph]].
- [9] M. Sekulla Ph.D. thesis, University of Siegen, 2015
- [10] M. Baak *et al.*, arXiv:1310.6708 [hep-ph].
- [11] C. Degrande *et al.*, arXiv:1309.7890 [hep-ph].
- [12] B. W. Lee, C. Quigg and H. B. Thacker, Phys. Rev. Lett. **38**, 883 (1977); Phys. Rev. D **16**, 1519 (1977).
- [13] J. Reuter and M. Tonini, JHEP **1302**, 077 (2013) [arXiv:1212.5930 [hep-ph]]. J. Reuter, M. Tonini and M. de Vries, arXiv:1307.5010 [hep-ph]; JHEP **1402**, 053 (2014) [arXiv:1310.2918 [hep-ph]].
- [14] M. Fierz and W. Pauli, Proc. Roy. Soc. Lond. A **173** (1939) 211.
- [15] E. C. G. Stueckelberg, Helv. Phys. Acta **11**, 225 (1938).
- [16] E. C. G. Stueckelberg, Helv. Phys. Acta **15** (1942) 23.
- [17] W. Kilian, T. Ohl and J. Reuter, *WHIZARD: Simulating Multi-Particle Processes at LHC and ILC*, Eur. Phys. J. C **71**, 1742 (2011) [arXiv:0708.4233 [hep-ph]].
- [18] M. Moretti, T. Ohl and J. Reuter, *O'Mega: An Optimizing matrix element generator*, In *2nd ECFA/DESY Study 1998-2001* 1981-2009 [hep-ph/0102195].
- [19] W. Kilian, T. Ohl, J. Reuter and C. Speckner, JHEP **1210**, 022 (2012) [arXiv:1206.3700 [hep-ph]].
- [20] W. Kilian, J. Reuter, S. Schmidt and D. Wiesler, JHEP **1204**, 013 (2012) [arXiv:1112.1039 [hep-ph]].
- [21] N. D. Christensen, C. Duhr, B. Fuks, J. Reuter and C. Speckner, Eur. Phys. J. C **72**, 1990 (2012) [arXiv:1010.3251 [hep-ph]].

- [22] B. Chokoufe Nejad, W. Kilian, J. Lindert, S. Pozzorini, J. Reuter, C. Weiss, in preparation; B. Chokoufe Nejad, W. Kilian, J. Reuter and C. Weiss, PoS EPS **-HEP2015**, 317 (2015) [arXiv:1510.02739 [hep-ph]]; C. Weiss, B. Chokoufe Nejad, W. Kilian and J. Reuter, PoS EPS **-HEP2015**, 466 (2015) [arXiv:1510.02666 [hep-ph]]; N. Greiner, A. Guffanti, T. Reiter and J. Reuter, Phys. Rev. Lett. **107**, 102002 (2011) [arXiv:1105.3624 [hep-ph]]; T. Binoth, N. Greiner, A. Guffanti, J. Reuter, J.-P. Guillet and T. Reiter, Phys. Lett. B **685**, 293 (2010) [arXiv:0910.4379 [hep-ph]]; W. Kilian, J. Reuter and T. Robens, Eur. Phys. J. C **48**, 389 (2006) [hep-ph/0607127].
- [23] H. Baer et al., arXiv:1306.6352 [hep-ph].
- [24] T. Behnke et al., arXiv:1306.6329 [physics.ins-det].
- [25] M. Beyer, W. Kilian, P. Krstonosic, K. Mönig, J. Reuter, E. Schmidt and H. Schröder, Eur. Phys. J. C **48**, 353 (2006) [hep-ph/0604048].
- [26] C. Fleper, W. Kilian, J. Reuter, M. Sekulla, in preparation.